Electronic Supplementary Material (ESI) for Lab on a Chip.

Supplementary Information

Smartphone fluorescent imaging-based mobile biosensing system integrated with passive fluidic control cartridge for minimal user intervention and high accuracy

Won-Il Lee[a], Younghyeon Park[d], Jaemin Park[e], Sajal Shrivastava[b], Young-Min Son[a], Hak-Jong Choi[f], Jaelin Lee[d], Byeungwoo Jeon[d], Heon Lee[*e], and Nae-Eung Lee[*abc]

[a]Samsung Advanced Institute for Health Sciences & Technology (SAIHST), Sungkyunkwan University, 2066 Seobu-ro, Jangan-gu, Suwon, Gyeonggi-do 16419, Korea

[b]School of Advanced Materials Science & Engineering, Sungkyunkwan University, 2066 Seobu-ro, Jangan-gu, Suwon, Gyeonggi-do 16419, Korea

[c]SKKU Advanced Institute of Nanotechnology (SAINT), Sungkyunkwan University, 2066 Seobu-ro, Jangan-gu, Suwon, Gyeonggi-do 16419, Korea

[d]Department of Electrical and Computer Engineering, Sungkyunkwan University, 2066 Seobu-ro, Jangan-gu, Suwon, Gyeonggi-do 16419, Korea

[e]Department of Material science and Engineering, Korea University, 145 Anam-ro, Seongbuk-gu, Seoul 02841, Korea

[f]Electrical & Systems Engineering, University of Pennsylvania, 200 South 33rd Street, Philadelphia, PA 19104

*Corresponding author; Nae-Eung Lee (E-mail: nelee@skku.edu), and Heon Lee (E-mail: nanoimprint@naver.com)

Method:

Image acquisition process

The sample value extraction of the fluorescence image can be affected by the method of image processing after being captured from the imaging sensor. Generally, the raw data captured by the image sensor consists of a single channel of two-dimensional mosaicked image according to the color filter array (CFA), which is attached in front of the sensor. After capturing the raw data, the final output image is created through the ISP inside the imaging device. In the ISP, representative image processing algorithms such as demosaicking, white balancing, color space conversion, noise reduction, and compression are processed sequentially [1]. The final output image produced after the ISP process is optimized to watch from the display system. However, the algorithms in the ISP may affect the value of measurement because the color conversion and compression processes are based on a human visual system, which increases the perceptual quality of the image. Besides, the compression by standard image coding such as JPEG [2] causes an information loss due to the quantization that degrades the quality of image.

In this study, the proposed method simplifies the processes in the ISP by performing only the demosaicking and grayscale conversion. In the demosaicking process, the single-channel raw data are converted into three channels of RGB data. In the grayscale conversion, a gray image is created by averaging the values of the three channels.

Demosaicking: After capturing from the image sensor, the mosaic patterns appear in the raw data due to the CFA in front of the sensor. To obtain a colored image from the raw data, a demosaicking process is necessary. In this study, the three-channel image is created by a bilinear interpolation-based demosaicking method.

Grayscale conversion: To measure a representative sample value from the three-channel image, grayscale conversion is performed in this study. The single-channel gray image can be derived by the following equation:

$$d_{gray}(i,j) = \frac{d_r(i,j) + d_g(i,j) + d_b(i,j)}{3}$$

where *i* and *j* are the horizontal and vertical indices in the image respectively, whereas $d_{gray}()$, $d_r()$, $d_g()$, and $d_b()$ are the pixel values of gray, red, green, and blue channels respectively.

ROI search: The place of the circle after the capture from the camera can be moved a little bit by the gap between the cartridge and mounting device. To measure the exact place within the circle, searching of ROI is necessary. In this study, the center position of the circle is calculated by the proposed ROI search method. There are two representative methods of finding the center of the circle. The first one is accumulating each horizontal and vertical axis of the image, respectively. After accumulation of each axis, the index at maximum value of each accumulated axis is determined by the center of the circle. The second method is based on convolution by applying the image with a binary circle mask, which has a value of 0 and 1. After the convolution process, the most correlated position (the maximum value) is determined by the center of the circle. These two methods have advantages and disadvantages. The accumulation method is relatively faster than the convolution-based method in that the computational complexity is $O(MN)$, where M and N are the horizontal and vertical sizes of the image, respectively. However, if the image has a lot of noise at the outside of the circle, the center position is not accurate. The convolution method is relatively accurate than the accumulation method on a noisy image. However, the complexity is much higher by $O(W^2R^2)$, where W is the size of searching window in the convolution, and R is the size of circle mask.

To compensate for the drawbacks of the two methods, their combination is proposed in this study. The proposed ROI searching method consists of two steps: First, the initial center position is calculated by the accumulation method. Then, the center position is refined by the convolution method with a small size of search window.

The initial center position can be calculated as below:

$$i_{acc} = \operatorname*{argmax}_{i} \sum_{j=1}^{N} d_{gray}(i,j),\ subject\ to\ i \in \{i, \dots, M\}$$

$$j_{acc} = \operatorname*{argmax}_{j} \sum_{i=1}^{M} d_{gray}(i,j),\ subject\ to\ j \in \{i, \dots, N\}$$

where i_{acc} and j_{acc} are the indices of initial center position, whereas M and N are the sizes of the horizontal and vertical axes of gray image, respectively. The initial center position is refined by the following 2D convolution:

$$[\mathrm{i}_{center}, \mathrm{j}_{center}] = \operatorname*{argmax}_{i,j} \sum_{k=0}^{R-1}\sum_{l=0}^{R-1} d_{mask}(k+1, l+1)d_{gray}(i+k, j+l),$$

subject to $i \in \left[i_{acc} - \frac{W}{2}, i_{acc} + \frac{W}{2}\right],\ j \in [j_{acc} - \frac{W}{2}, j_{acc} + \frac{W}{2}]$

where i_{center} and j_{center} are the center positions, k and l are the indices of mask image, and R is the horizontal and vertical size of mask image. W is the size of searching window in the convolution process.

Measurement: After finding the center position of ROI, measurement of the value in the ROI is conducted. The shape of the ROI range is circular and the pixel indices in the ROI range can be derived using the following equation:

$$i_{ROI} \in [i_{center} - \frac{R}{2}, i_{center} + \frac{R}{2}]$$

$$j_{ROI} \in [j_{center} - \frac{R}{2}, j_{center} + \frac{R}{2}],\ subject\ to\ \left(i_{ROI} - i_{center}\right)^2 + \left(j_{ROI} - j_{center}\right)^2 < \left(\frac{R}{2}\right)^2$$

The sample value is measured by the sum of the pixel values in the ROI:

$$SampleVal = \sum_{i \in i_{ROI}} \sum_{j \in j_{ROI}} d_{grey}(i,j)$$

where *SampleVal* is the measured value from the image.

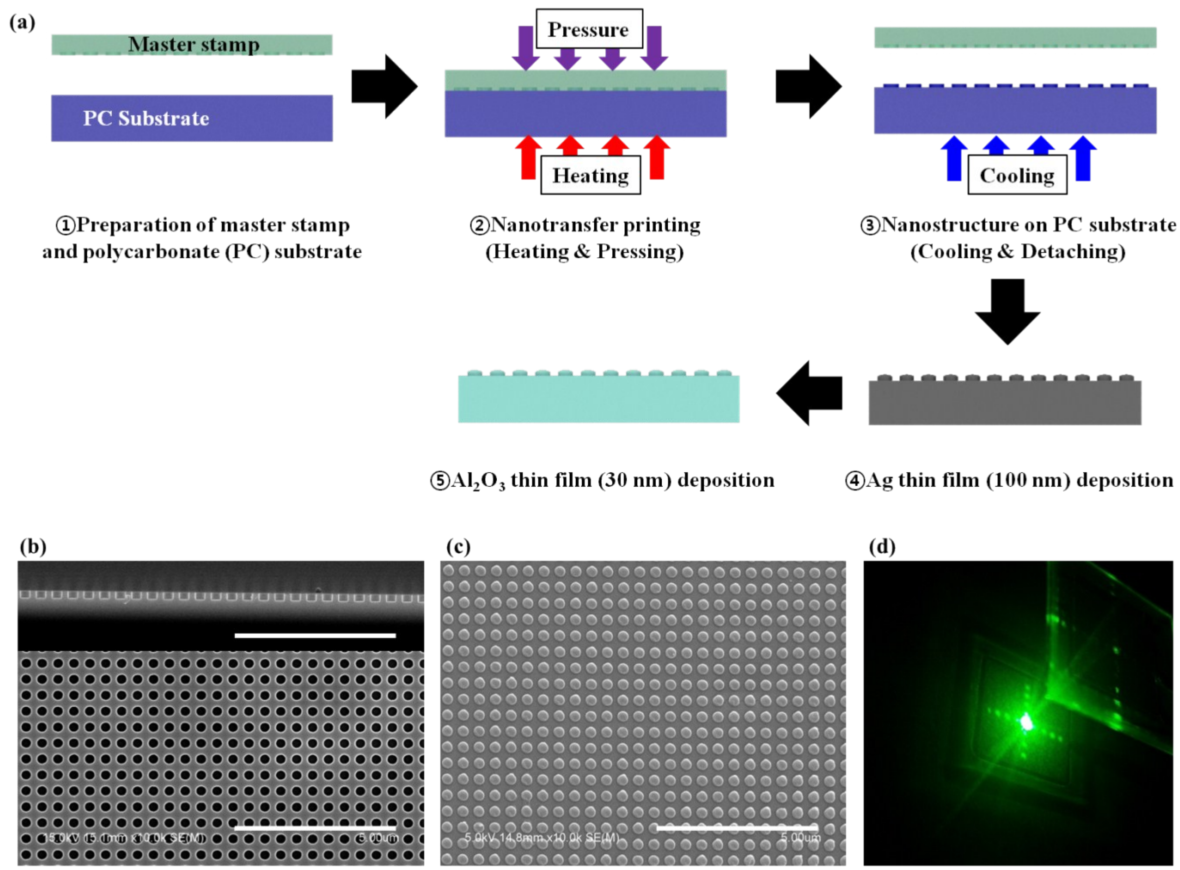

Fig. S1. Preparation of nanometalized substrate for metal-enhanced fluorescence. (a) Schematic of fabrication of nanometalized PC substrate. (b) FESEM image of master stamp in the top view and cross-section (inset) (scale bar: 5 µm). (c) Hot-embossed PC substrate with nanopillar structure (scale bar: 5 µm). (d) Confirmation of nanopillar array over the hot-embossed area on PC substrate with laser diffraction pattern.

(a)

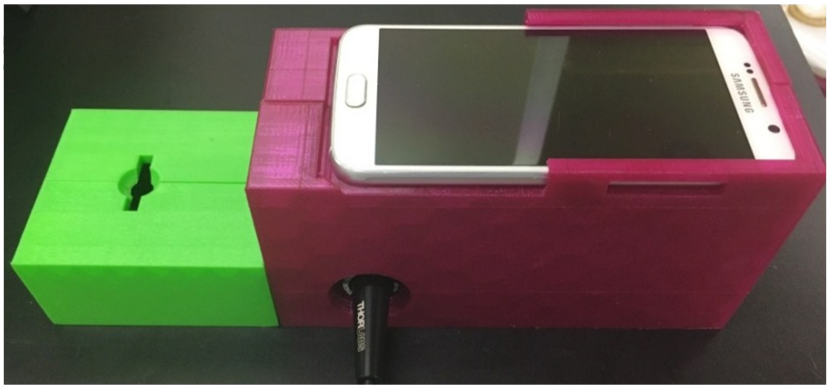

(b)

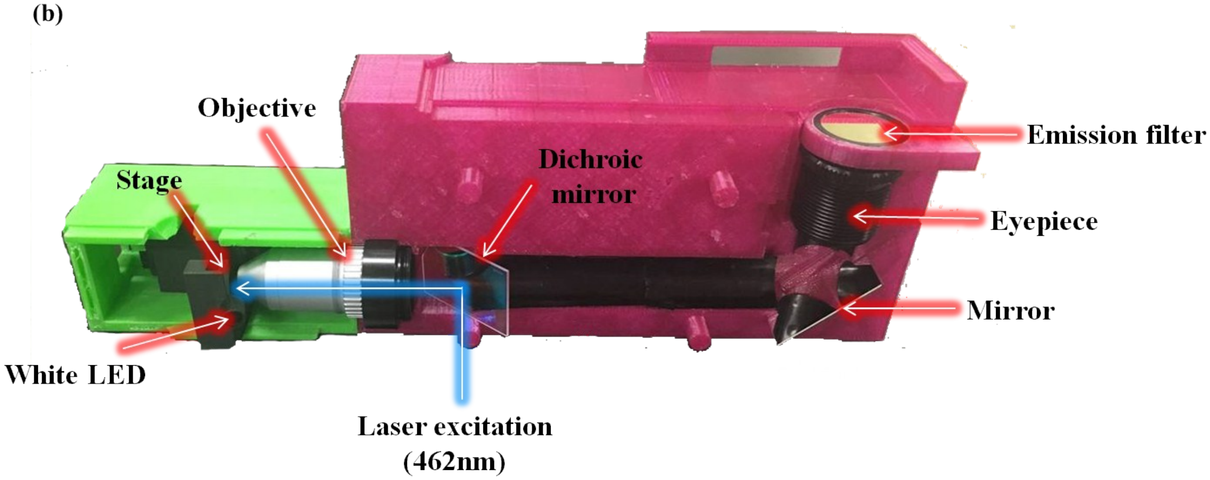

Fig. S2. Photograph of (a) SFM appearance and (b) its inside composition.

(a)

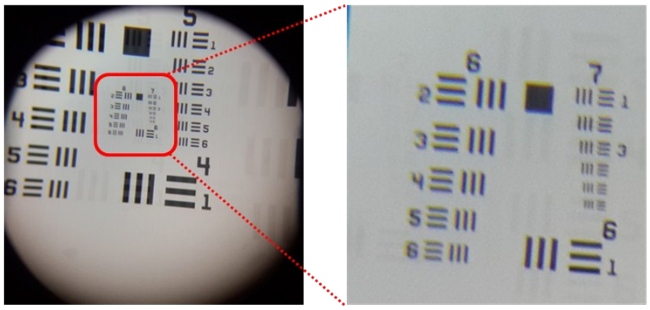

1951 USAF resolution test target

No.	Group6 (lp/mm)	spacing (μm)	Group7 (lp/mm)	spacing (μm)
1	64	7.8	128	3.9
2	71.8	6.96	144	3.4
3	80.6	6.2	161	3.1
4	90.5	5.5	181	**2.76**
5	102	4.9	203	**2.46**
6	114	4.4	228	**2.19**

(b)

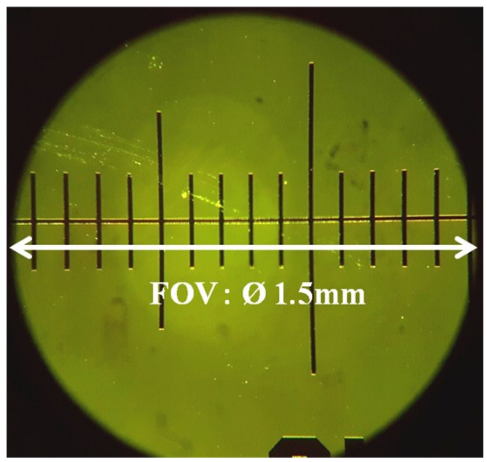

Fig. S3. Optical microscope image of SFM. (a) Resolution of the image reaches No. 6 at group 7 of 1951 USAF resolution test target. (b) Field of view is 1.5 mm at diameter metered by stage micrometer with 100 μm division.

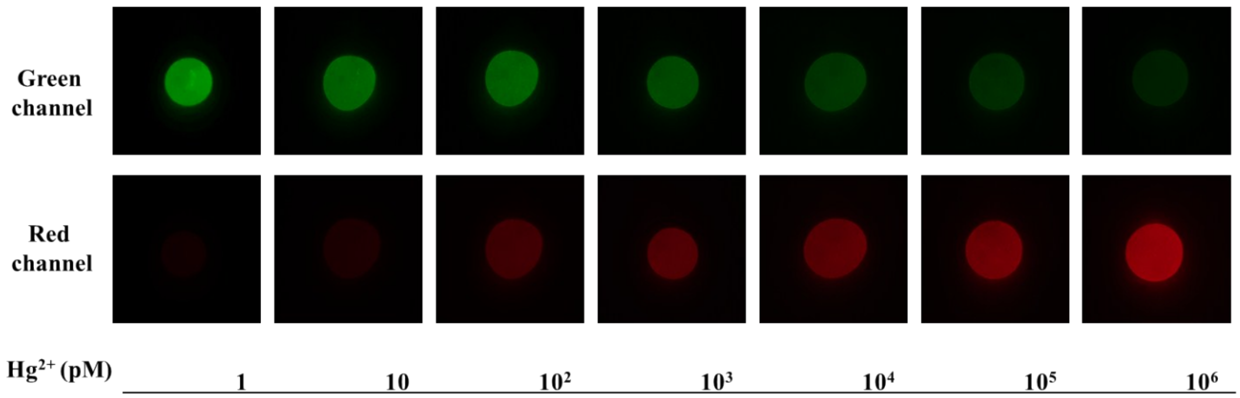

Fig. S4. Quantitative fluorescent images vs. Hg^{+} concentration at green and red channels obtained by SFM.

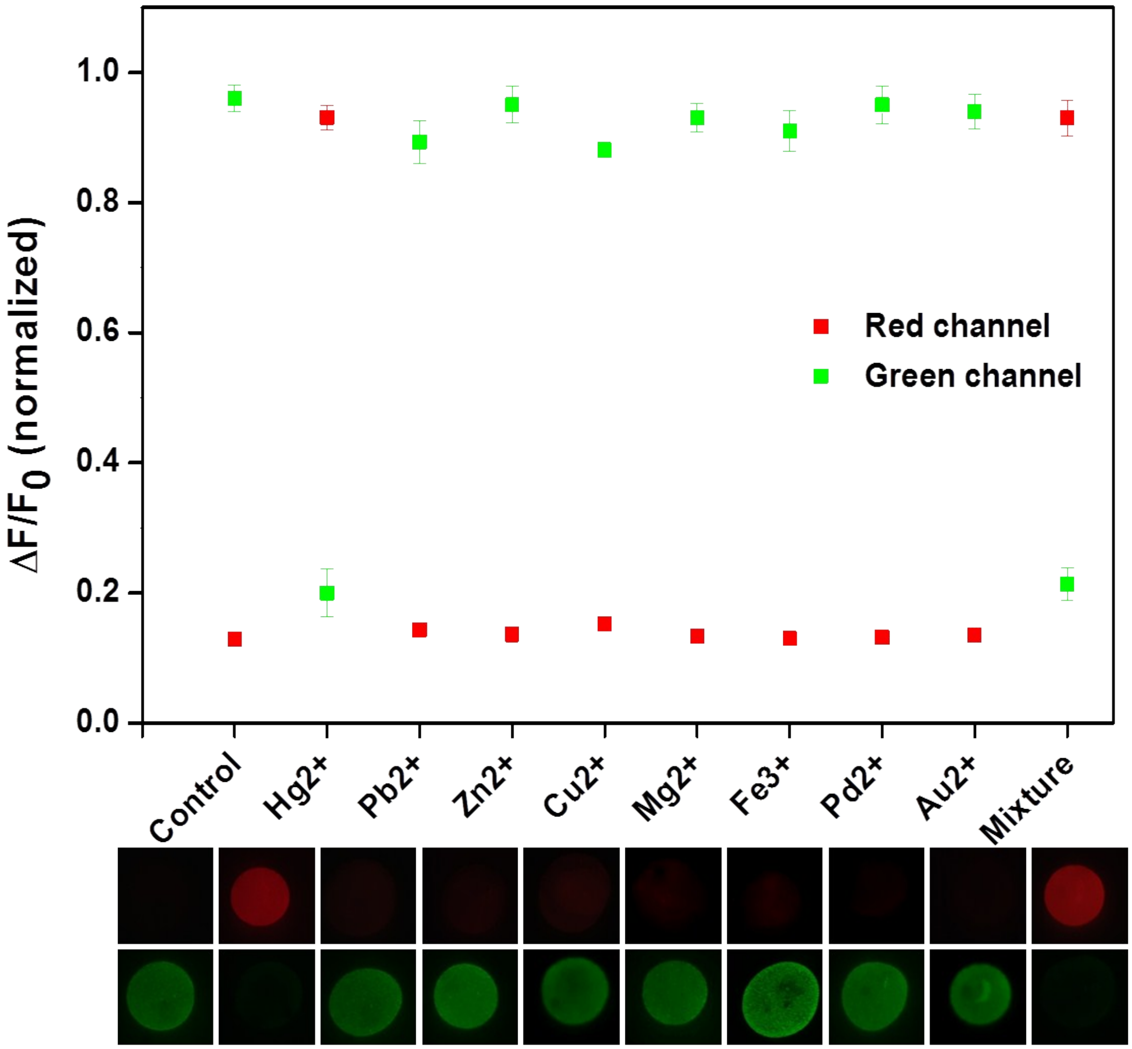

Fig. S5. Selectivity test for Hg^{2+} with various metal ions (1 μM)

Table S1. Assay validation using Hg^{2+} spiked wastewater samples

Sample No. (n=3)	Spiked Hg^{2+} (nM)	CVAAS			Smartphone fluorescence microscope (SFM)		
		Measured Hg^{2+} (nM)	Recovery (%)	RSD (%)	Measured Hg^{2+} (nM)	Recovery (%)	RSD (%)
1	0	0	N.A.	N.A.	0	N.A.	N.A.
2	1	1	100	0.8	0.9	94	14.6
3	2.5	2.5	100	2	2.7	107	13.2
4	5	5	100	2	6.1	121	10
5	7.5	7.5	100	6.3	8.6	115	14.9
6	10	10	100	4.7	10.2	102	14.3
7	12.5	12.5	100	2	10.9	87	13.4
8	15	14.5	97	6.9	16.7	111	14
9	25	25	100	2	21.9	88	9.5
10	50	48.9	98	2.2	55.8	112	9.2

Movie S1. The actual operation of the cartridge over time

Movie S2. A simple washing step after purging

References:

1. R. Lukac, *Single-Sensor Imaging: Methods and Applications for Digital Cameras*, CRC Press, 2008.
2. G. K. Wallace, *IEEE Transactions on Consumer Electronics*, 1992, **38**, xviii-xxxiv.